International Journal of Applied Engineering Research ISSN 0973-4562 Volume 14, Number 14 (2019) pp. 3123-3132

Investigation of the Effect of Directivity Pulses on the Seismic Response of a Curved RC Bridge

Vassiliki Kardoutsou*, Vasileios Angelidakis, Ioannis Psycharis, Ioannis Taflampas

School of Civil Engineering, National Technical University of Athens, Heroon Polytechneiou 9, Zografou 15780, Greece.

Abstract

Within the near-fault zone, ground motions are influenced by the rupture mechanism and directivity phenomena. Near-fault ground motions are of special interest in Earthquake Engineering, as they might result in large inelastic displacements of structures. In this paper, an investigation is presented concerning the effect of the directivity pulses inherent in near-fault ground motions on the inelastic response of a curved RC bridge, specifically Bridge G7 of Egnatia Highway in Greece. The analyses were performed for a sample of 90 near-fault seismic records. From each record, the first six pulses were extracted and simplified 'pulse records' were defined, composed of one or more (up to six) pulses. First, a pushover analysis was performed and, based on the derived yield acceleration corresponding to the bilinear representation of the capacity curve, each record was scaled to three intensity levels, corresponding to behavior factors q_y = 2, 3 and 4. Non-linear time-history analyses were then performed for each original record and the related 'pulse records' using OpenSees. By comparing the results, conclusions were drawn on the significance of each pulse to the nonlinear response. To this end, the errors for several general and local response quantities were calculated. The results show that the maximum inelastic deformations occur for the ground motions for which the elastic fundamental period of the bridge is close to one half of the period of the predominant pulse. Also, in most cases, the maximum response for the original record could be adequately estimated by the response for the 'pulse record' consisted of only two (and in few cases of three) pulses, especially when the fundamental period of the bridge was in between the periods of these pulses.

Keywords: Near-fault; Directivity pulse; Nonlinear response; Time-history analysis; Synthetic ground motions; Bridges.

INTRODUCTION

A characteristic feature of near-fault ground motions is the appearance of discrete directivity pulses inherent in the ground motion time-histories, which are evidently pronounced in the ground velocity time-history. Ground motions affected by forward directivity effects of near-source seismic events have been the subject of systematic studies in the last decades. Several researchers have isolated the most significant characteristics of the seismic action near active faults and their effect on the elastic and inelastic response, mainly for *SDOF* systems. In what concerns the elastic response, Shahi and Baker [1] observed a bell-shaped amplification of the elastic spectral values around the period of the predominant pulse, T_p. For inelastic response, Tothong and Cornell [2] observed increased values of the ductility to the behavior factor ratio, μ/q, for structures with period around one half of the period of the predominant pulse.

In this paper, an extension of this investigation to include not only the predominant pulse, but also other significant pulses (up to six) inherent in near-fault ground motions, is presented. Analyses were performed for a more complex structure, specifically a curved bridge, for a sample of 90 near-fault seismic records classified as pulse-like in the literature.

It is reminded that, as common practice (Mavroeidis and Papageorgiou [3], Baker [4]), the identification and the extraction of the significant directivity pulses is performed through wavelet analyses, using idealized wavelet forms for their mathematical representation. In the present investigation, the Mavroeidis and Papageorgiou [3] wavelet was used for the representation of the six most significant pulses in each record, which were identified by applying the Mimoglou *et al.* [5] methodology.

It should be noted that recent studies have proposed the approximation of near-fault ground motions by synthesized records constructed from the superposition of idealized pulses (Lu and Panagiotou [6]). To this end, this study was focused on the number of significant pulses required to adequately estimate the inelastic response of the considered bridge, compared with the non-linear time history (NLTH) response for the original record.

Structure considered

All the analyses were performed for the case study of an existing curved three-span bridge, specifically Bridge G7 of Egnatia Highway, Greece. The overall length of the bridge is 270.00 m, consisting of two end spans of 75.00 m each and a central span of 120.00 m. In plan, the bridge lies on a circular arc of radius 320 m. Vertically, the red line of the highway forms a arc of radius 1000 m, which creates a height difference of 6.5 m between the end sections of the deck. A general view of the bridge is presented in Fig. 1.

* Corresponding author.
E-mail address: vkardcv@gmail.com

The deck is connected monolithically to the mid-piers and has a heavily post-tensioned single-cell box cross section of variable height. The height mid-piers M1 and M2 41.70 m and 49.50 m, respectively, and share a hollow rectangular cross section with outer dimensions of 4.00 m × 7.35 m and thickness 0.75 m. Typical cross sections of the deck and the piers are presented in Fig. 2. Both the deck and the piers are made of concrete C35/45. The reinforcement is of grade S500s and the number of the longitudinal rebars of the piers is consistent throughout their height and equal to 252 Ø28 ($\rho \approx$ 1.05%).

The deck is supported by the abutments through elastic single-point pot bearings, which allow its free sliding the longitudinal direction, while, in the transverse direction, the motion of the deck is restrained by shear keys, which, however, break for seismic loads larger than the design ones.

The piers are founded on circular concrete shafts of diameter 10.00 m and height 15.00 m.

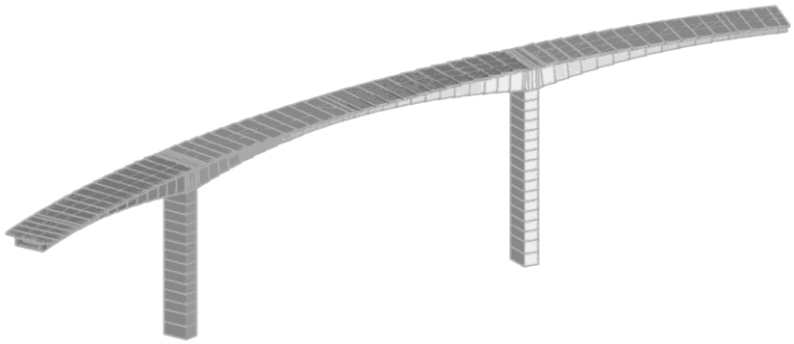

Fig. 1: General view of the bridge considered in the analyses.

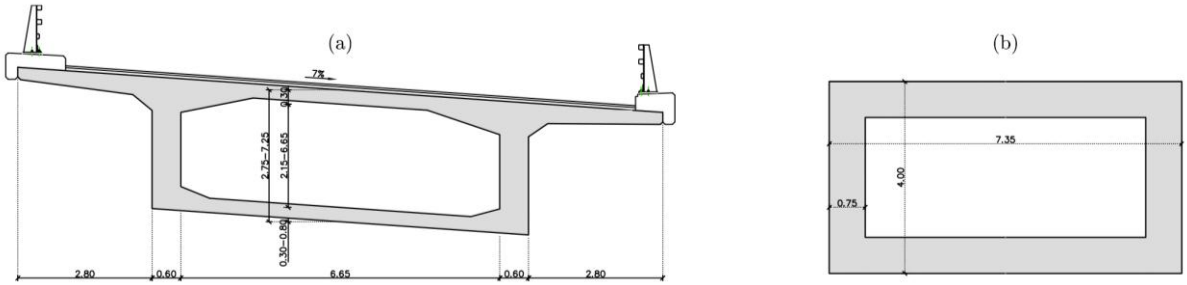

Fig. 2: Typical cross sections (a) Deck, (b) Piers.

NUMERICAL MODEL

The structure was simulated in the open-source software OpenSees [6]. The deck of the bridge was modelled using Elastic Beam-Column Elements, since formation of plastic hinges is expected only at the piers.

The piers M1 and M2 were supposed fixed at their base, considering the foundation type and the rocky soil conditions. For their modelling, force-based beam-column elements were used. The fibers of the sections were assigned with uniaxial material constitutive laws, which defined their monotonic and cyclic behavior. The formation of plastic hinges at their ends was simulated using the distributed plasticity model, in order to simulate the gradual spread of plasticity along the piers' and the sections' height and thus, approximate the real behavior in an optimum way.

Mean values for the strength of the materials were considered, as typical in non-linear analyses. In **Fig. 3**, the discretization of a typical fiber section of the piers is presented.

The behavior of the reinforcing steel was simulated using the Steel02 material of OpenSees, which describes a Menegotto-Pinto [8] steel material. The cover-concrete inside and outside the confined cores of each section was simulated using the Concrete01 material of OpenSees, which creates a Kent-Park stress-strain curve, as it was modified by Scott *et al*. [9]. Zero residual strength was considered, in order to simulate the spalling of the cover concrete. The confined concrete was simulated using the Concrete04 material of OpenSees, which creates a Popovic [10] stress-strain material. The characteristics of the confined concrete were computed using the stress-strain model proposed by Mander *et al*. [11], who also used the Popovic stress-strain curve in their studies. Due to different transverse reinforcement spacing along the height of the piers, and consequently the provided lateral confining stress, three different cases of confined concrete were defined, as shown in Fig. 4(a).

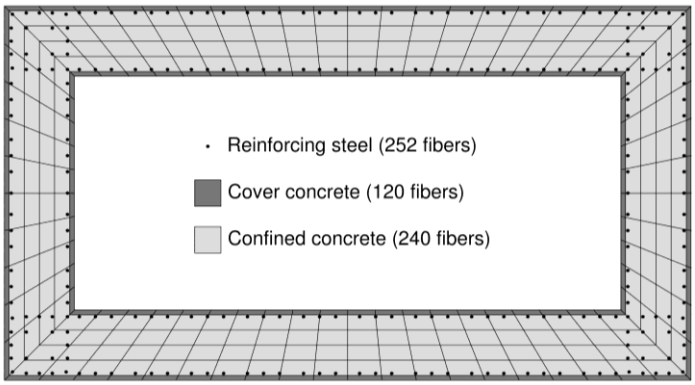

Fig. 3: Typical fiber section of the piers.

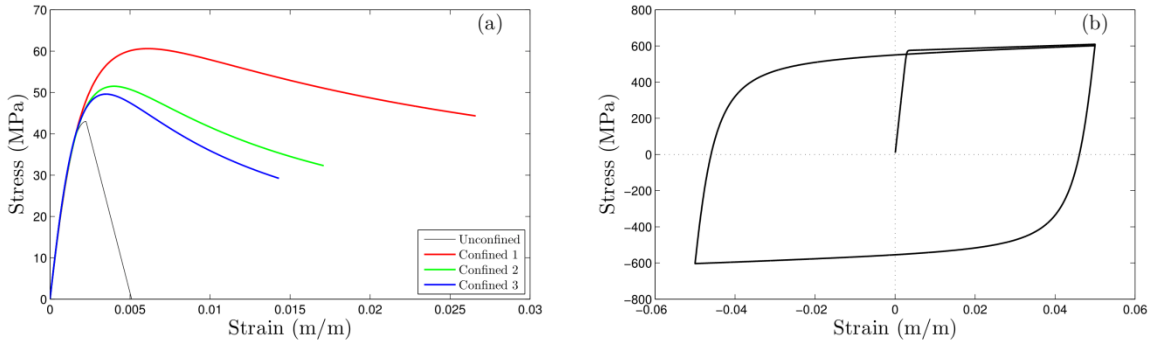

Fig. 4: Constitutive laws used to model the behavior of the materials: (a) Monotonic behavior for the cover and the confined cores' concrete material; (b) Cyclic behavior of the reinforcing steel material.

The abutments A1 and A2 were considered rigid in their long direction (transverse direction of the bridge), due to the corresponding large stiffness. Thus, and taking under consideration the free sliding in the longitudinal direction of the bridge, the abutments were not included in the model of the structure; instead, appropriate boundary conditions were applied at the ends of the bridge: free sliding in the longitudinal direction and restriction of motion in the transverse and the vertical directions, due to the presence of the shear keys; the latter were modeled as Zero-Length Elements with very large elastic stiffness, acting in the normal to the axis of the bridge direction. It must be noted that due to the plan curvature of the deck and the existence of shear keys at the abutments, the transverse and longitudinal displacements are partially interacting, resulting to biaxial bending conditions at the piers, for every horizontal movement of the deck.

The superstructure, apart from its dead weight, bears additional dead loads of 42.0 kN/m and traffic loads equal to 44.0 kN/m. For the latter, a load combination coefficient ψ_2 = 0.20 was used to calculate the corresponding mass.

Static Pushover Analysis

Firstly, the main features of the inelastic behavior of the structure were assessed from the capacity curve computed through a Static Pushover (SPO) Analysis. Throughout this paper, only the response of the bridge in the longitudinal direction is considered, thus, the SPO analysis was performed for horizontal loads according to the dominant eigenmode in this direction. From the corresponding capacity spectrum the idealized bilinear (elastic-perfectly plastic) behavior was derived (Fig. 5) following the FEMA 273 [12] procedure and the yield parameters of the equivalent *SDOF* system we determined: yield acceleration S_{ay} = 1.811 m/s^2, yield displacement S_{dy} = 0.225 m and elastic period T^* = 2.215 s.

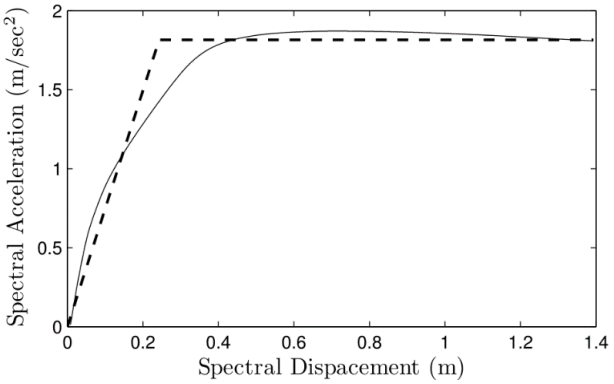

Fig. 5: Capacity Spectrum of the equivalent *SDOF* system (longitudinal direction).

Ground motions and corresponding pulses

A sample of 90 near-fault seismic records of magnitude ranging from M_w = 5.0 to 7.4 was selected for the analyses. From these, 55 were classified as pulse-like by Baker [4], while the rest 35 were classified as pulse-like by Kardoutsou *et al*. [13]. The list of the considered records is shown in Table 1, while their elastic pseudo-acceleration response spectra for 5% damping, normalized with respect to the peak ground acceleration (*PGA*) of each record, are presented in Fig. 6.

Table 1. Seismic Records

#	Event	Year	Station	PGV (cm/sec)	M_w
1	San Fernando	1971	Pacoima Dam (upper left abut)	116.50	6.60
2	Coyote Lake	1979	Gilroy Array #6	51.50	5.70
3	Imperial Valley-06	1979	Aeropuerto Mexicali	44.30	6.50
4	Imperial Valley-06	1979	Agrarias	54.40	6.50
5	Imperial Valley-06	1979	Brawley Airport	36.10	6.50
6	Imperial Valley-06	1979	EC County Center FF	54.50	6.50
7	Imperial Valley-06	1979	EC Meloland Overpass FF	115.00	6.50
8	Imperial Valley-06	1979	El Centro Array #10	46.90	6.50
9	Imperial Valley-06	1979	El Centro Array #11	41.10	6.50
10	Imperial Valley-06	1979	El Centro Array #3	41.10	6.50
11	Imperial Valley-06	1979	El Centro Array #4	77.90	6.50
12	Imperial Valley-06	1979	El Centro Array #5	91.50	6.50
13	Imperial Valley-06	1979	El Centro Array #6	111.90	6.50
14	Imperial Valley-06	1979	El Centro Array #7	108.80	6.50
15	Imperial Valley-06	1979	El Centro Array #8	48.60	6.50
16	Imperial Valley-06	1979	El Centro Differential Array	59.60	6.50
17	Imperial Valley-06	1979	Holtville Post Office	55.10	6.50
18	Mammoth Lakes-06	1980	Long Valley Dam (Upr L Abut)	33.10	
19	Irpinia, Italy-01	1980	Sturno	41.50	6.90
20	Westmorland	1981	Parachute Test Site	35.80	5.90
21	Coalinga-05	1983	Oil City	41.20	
22	Coalinga-05	1983	Transmitter Hill	46.10	
23	Coalinga-07	1983	Coalinga-14th & Elm (Old CHP)	36.10	
24	Morgan Hill	1984	Coyote Lake Dam (SW Abut)	62.30	6.20
25	Morgan Hill	1984	Gilroy Array #6	35.40	6.20
26	Taiwan SMART1(40)	1986	SMART1 C00	31.20	6.10
27	Taiwan SMART1(40)	1986	SMART1 M07	36.10	6.10
28	N. Palm Springs	1986	North Palm Springs	73.60	6.10
29	San Salvador	1986	Geotech Investig Center	62.30	5.80
30	Whittier Narrows-01	1987	Downey - Co Maint Bldg	30.40	6.00
31	Whittier Narrows-01	1987	LB - Orange Ave	32.90	6.00
32	Superstition Hills-02	1987	Parachute Test Site	106.80	6.50
33	Loma Prieta	1989	Alameda Naval Air Stn Hanger	32.20	6.90
34	Loma Prieta	1989	Gilroy Array #2	45.70	6.90

#	Event	Year	Station	PGV (cm/sec)	M_w
35	Loma Prieta	1989	Oakland - Outer Harbor Wharf	49.20	6.90
36	Loma Prieta	1989	Saratoga - Aloha Ave	55.60	6.90
37	Erzican, Turkey	1992	Erzincan	95.40	6.70
38	Cape Mendocino	1992	Petrolia	82.10	7.00
39	Landers	1992	Barstow	30.40	7.30
40	Landers	1992	Yermo Fire Station	53.20	7.30
41	Northridge-01	1994	Jensen Filter Plant	67.40	6.70
42	Northridge-01	1994	Jensen Filter Plant Generator	67.40	6.70
43	Northridge-01	1994	LA - Wadsworth VA Hospital North	32.40	6.70
44	Northridge-01	1994	LA Dam	77.10	6.70
45	Northridge-01	1994	Newhall - W Pico Canyon Rd.	87.80	6.70
46	Northridge-01	1994	Pacoima Dam (downstr)	50.40	6.70
47	Northridge-01	1994	Pacoima Dam (upper left)	107.10	6.70
48	Northridge-01	1994	Rinaldi Receiving Sta	167.20	6.70
49	Northridge-01	1994	Sylmar - Converter Sta	130.30	6.70
50	Northridge-01	1994	Sylmar - Converter Sta East	116.60	6.70
51	Northridge-01	1994	Sylmar - Olive View Med FF	122.70	6.70
52	Kobe, Japan	1995	Takarazuka	72.60	6.90
53	Kobe, Japan	1995	Takatori	169.60	6.90
54	Northwest China-03	1997	Jiashi	37.00	6.10
55	Yountville	2000	Napa Fire Station #3	43.00	5.00
56	Friuli, Italy	1976	Gemona E	68.33	5.90
57	Friuli, Italy	1976	Gemona N	33.71	5.90
58	L' Aquila, Central Italy	2009	L'Aquila-V.Aterno-Aquil Parking. E	32.05	6.30
59	L' Aquila, Central Italy	2009	L'Aquila-V.Aterno-Aquil Parking. N	35.66	6.30
60	L' Aquila, Central Italy	2009	L'Aquila-V.Aterno- F.Aterno E	31.77	6.30
61	NW Balkan Peninsula, Montenegro	1979	Bar-Skupstina Opstine E	50.41	6.90
62	Kerman, Southern Iran	2003	Bam	120.42	6.60
63	Kerman, Southern Iran	2003	Bam	63.59	6.60
64	Kerman, Southern Iran	2003	Bam	39.73	6.60
65	Erzincan, Turkey	1992	AI_178_ERC_MET E	76.62	6.60
66	Erzincan, Turkey	1992	AI_178_ERC_MET N	108.41	6.60
67	Izmit, Turkey	1999	AI_199_TPT E	62.65	7.40
68	Duzce, Turkey	1999	AI_011_DZC E	82.65	7.00
69	Duzce, Turkey	1999	AI_011_DZC N	68.05	7.00
70	Bingl, Turkey	1999	AI_049_BNG N	34.14	6.40
71	Emilia Romagna, Northern Italy	2012	Mire E	27.45	6.00
72	Emilia Romagna, Northern Italy	2012	Mire N	58.46	6.00
73	Emilia Romagna, Northern Italy	2012	Mirh E	24.68	6.00

#	Event	Year	Station	PGV (cm/sec)	M_w
74	Emilia Romagna, Northern Italy	2012	Mirh N	55.02	6.00
75	Emilia Romagna, Northern Italy	2012	Mirandola (Napoli) E	28.45	6.00
76	Emilia Romagna, Northern Italy	2012	Mirandola (Napoli) N	57.46	6.00
77	Emilia Romagna, Northern Italy	2012	San Felice Sur Parano E	19.59	6.00
78	Emilia Romagna, Northern Italy	2012	San Felice Sur Parano N	35.22	6.00
79	Emilia Romagna, Northern Italy	2012	T0802 E	16.97	6.00
80	Emilia Romagna, Northern Italy	2012	T0802 N	24.37	6.00
81	Emilia Romagna, Northern Italy	2012	T0818 N	39.18	6.00
82	Emilia Romagna, Northern Italy	2012	Medolla E	31.29	6.00
83	Emilia Romagna, Northern Italy	2012	Medolla N	52.33	6.00
84	Emilia Romagna, Northern Italy	2012	Mirandola MRN N	53.37	6.00
85	Emilia Romagna, Northern Italy	2012	Quarantoly 2 N	32.42	6.00
86	Izmit, Turkey	1999	AI_004_IZT E	38.40	7.40
87	Emilia Romagna, Northern Italy	2012	Mirandola MRN E	36.29	6.00
88	Kefalonia, Greece	2014	Lixouri, O.T.E. E	115.26	6.00
89	Kefalonia, Greece	2014	Lixouri, O.T.E. N	80.52	6.00
90	Lefkada, Greece	2015	Vassiliki N	58.62	6.40

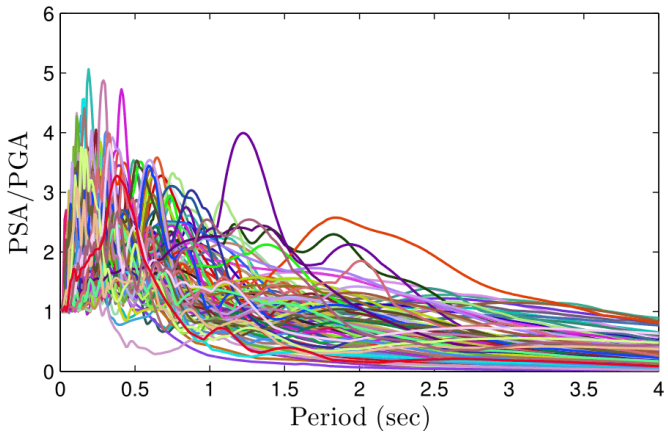

Fig. 6: Elastic Pseudo-Acceleration response spectra for 5% damping of the considered records, normalized with respect to their *PGA*.

For each ground motion, the first six significant pulses P_i (i=1 to 6) were extracted by applying the methodology described in Mimoglou *et al*. [5] and using the Mavroeidis & Papageorgiou [3] wavelet for the mathematical representation of the pulses. An example is presented for the EC County FF station record of the Imperial Valley, 1979 Earthquake. From the derived pulses (Fig. 7), six *pulse records* were constructed by superimposing them, specifically: (1) only the first pulse (denoted as S_1); (2) the first two pulses (denoted as S_2); (3) the first three pulses (denoted as S_3); …; (6) all six pulses (denoted as S_6). The pulse records for the above-mentioned ground motion are shown in Fig. 8.

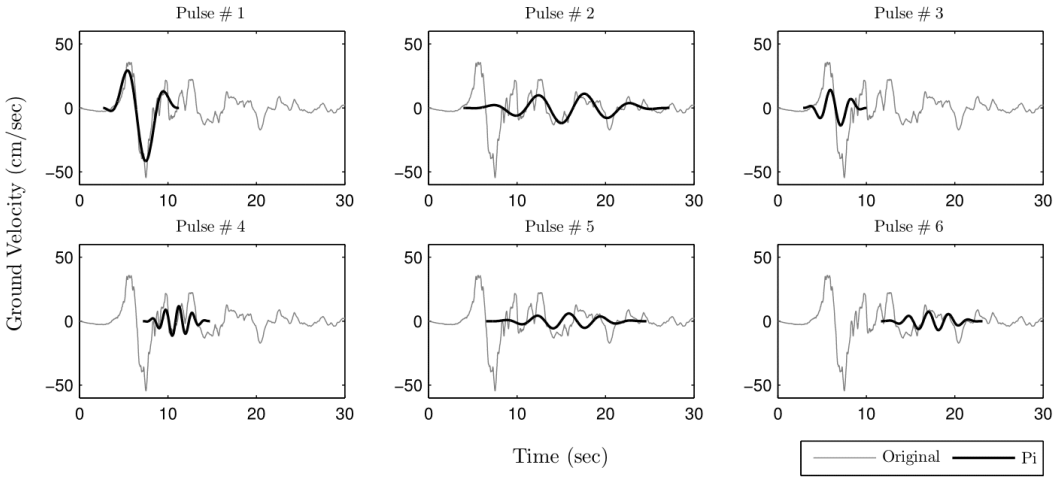

Fig. 7: Velocity time histories of the first six significant pulses (bolded lines) for the EC County FF station record of the Imperial Valley, 1979 Earthquake. The original record is shown with grey line.

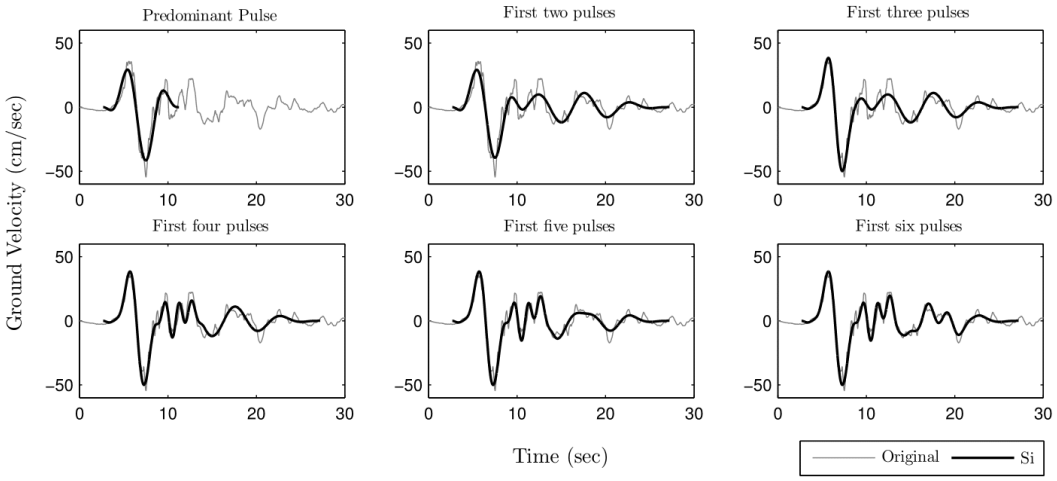

Fig. 8: Velocity time histories of the six corresponding pulse records (bolded lines) for the EC County FF station record of the Imperial Valley, 1979 Earthquake. The original record is shown with grey line.

Non-Linear Time-History Analyses

Scaling of the records

Analyses were performed for three intensity levels of each record. Specifically, each ground motion and its corresponding pulse records were scaled for values of the behavior factor q_y = 2, 3 and 4 using the following scaling factor, *SF*:

$$SF = q_y \cdot \frac{S_{ay}}{S_{a,el}(T^*)} \quad (1)$$

where S_{ay} and T^* are the yield acceleration and the period of the equivalent *SDOF* system, respectively, (derived in Section 4) and $S_{a,el}(T^*)$ is the elastic pseudo-acceleration for period $T=T^*$ and 5% damping that corresponds to the original record.

Maximum response quantities

In order to investigate the effect of directivity phenomena on the non-linear response and examine whether the original ground motions could be substituted by the simpler 'pulse records', at least in what concerns the estimation of the expected damage, the following response quantities, which are associated with damage, were examined:

The maximum ductility, μ, that develops during the seismic motion. The ductility is measured in terms of the equivalent *SDOF* system, by:

$$\mu = S_{du} / S_{dy} \quad (2)$$

where S_{du} is the displacement of the equivalent *SDOF* system that corresponds to the maximum displacement of the reference point of the bridge, as calculated from the NLTH analysis, and S_{dy} is the yield displacement of the equivalent *SDOF* system, as determined in Section 4.

The maximum drift ratios of the piers that develop during the seismic motion.

The maximum curvatures that develop during the seismic motion at the edge sections of the piers.

Results

The results obtained for the original records are presented in **Fig. 9**, in which the variation of the aforementioned quantities versus the period ratio T^*/T_{p1} is presented, with T_{p1} being the period of the predominant pulse of each record, which corresponds to the peak of the convolution spectrum $S_v \times S_d$ for 5% damping, as introduced by Mimoglou *et al.* [5]. The solid lines correspond to the moving average of the scattered data for each behavior factor q_y, produced through locally weighted regression analysis.

It is observed that the maximum inelastic response occurs when the period of the predominant pulse is double the period of the structure ($T^*/T_{p1} \approx 0.5$) and the minimum when $T_{p1} \approx T^*$. As shown in **Fig. 9**(a), for $T^*/T_{p1} \approx 0.5$ the required ductility μ is significantly larger than the corresponding behevior factor q_y, thus, the equal displacement rule does not hold. A similar conclusion was found by Tothong and Cornell [2] for *SDOF* structures.

As a second step, it was investigated whether the simplified 'pulse records' S_1 to S_6 could be used instead of the original records to produce similar maximum values of the examined response quantities. It is reminded that S_1 refers to the predominant pulse only, S_2 to the record produced by the superposition of the first two pulses, S_3 to the record produced by the superposition of the first three pulses, and so on. More specifically, the investigation aimed at finding the number of significant pulses that, if superposed into a 'pulse record', can adequately approximate the maximum response of the structure. The efficiency of each 'pulse record' S_i (i = 1 to 6) was measured from the produced error er_i (R_j) to the response quantity R_j, calculated by:

$$er_i = \frac{R_j(S_i) - R_j(orig)}{R_j(orig)} \qquad (3)$$

where R_j ($orig$) is the response quantity R_j calculated for the original record and R_j (S_i) the corresponding value calculated for the 'pulse record' S_i.

Moving averages of the errors produced by the use of 'pulse records' S_1, S_2, S_3 and S_6 in case of q_y = 4 versus the period ratio T^*/T_{p1} are presented in Fig. 10. The errors are shown with their absolute value, since it was observed that their sign did not follow any specific trend indicating underestimation or overestimation of the response. The respective graphs for intensity levels q_y = 2 and q_y = 3 are not presented, as they show similar behavior.

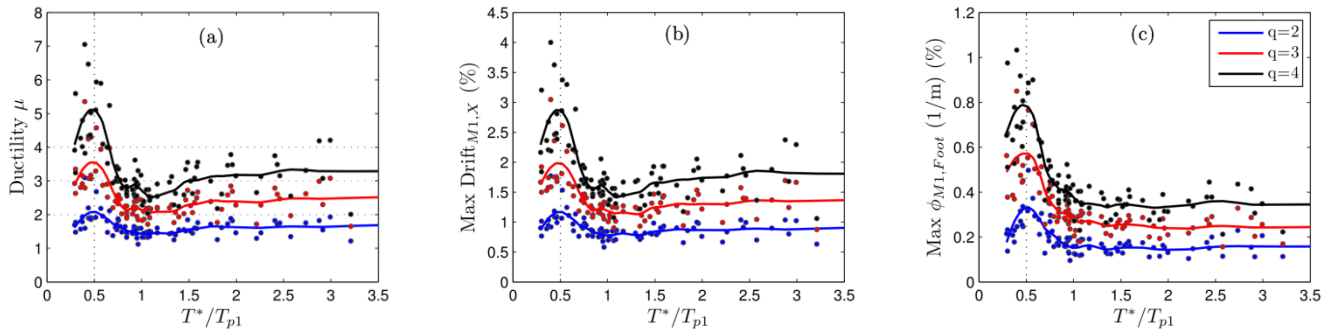

Fig. 9: Maximum response quantities of the structure for the three intensity levels: (a) Ductility of the equivalent *SDOF*; (b) Maximum drift of Pier M1; (c) Maximum Curvature at the base of pier M1. Solid lines correspond to the moving average of the obtained data.

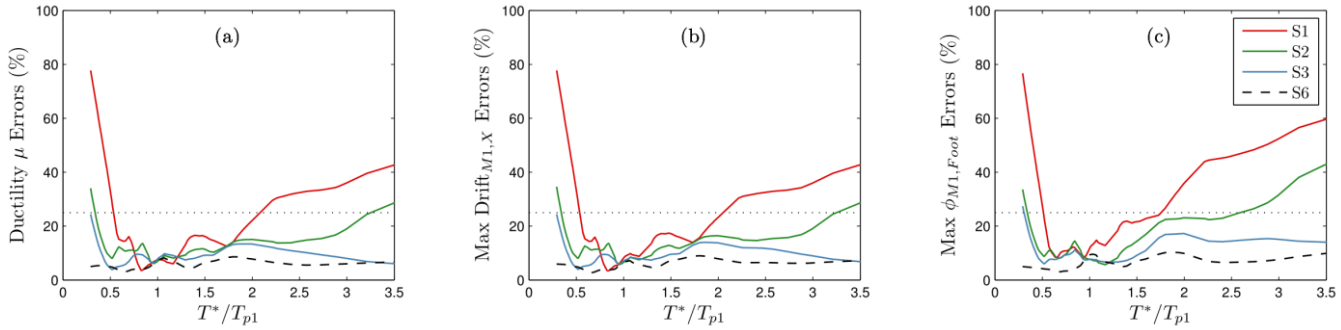

Fig. 10: Moving averages of the absolute values of the errors produced using pulse records S_1, S_2, S_3 and S_6 for q_y = 4: (a) Ductility of the equivalent *SDOF*; (b) Maximum drift of pier M1; (c) Maximum curvature at the base of pier M1.

Adopting an acceptable error level of 25% (shown with a dotted line on the graphs of Fig. 10), it is observed that the first pulse alone (record S_1) can adequately predict the maximum inelastic response if $0.6 < T^*/T_{p1} < 2.0$, i.e. if the period of the structure is larger than 60% of the period of the pulse and less than twice the pulse period. For structures with period outside this range, the produced error is significant. Thus, the first pulse alone cannot be unconditionally used as a sufficient 'pulse record', a conclusion that was also derived by Lu and Panagiotou [6].

If the second pulse is included in the 'pulse record' (S_2), the range of periods in which acceptable results are obtained increases significantly: errors less than 25% are obtained for $0.3 < T^*/T_{p1} < 3.0$. Interesting to note that the accuracy achieved for T^* close to T_{p1} does not improve.

Increasing even more the number of pulses considered (three or more) results in better accuracy only for large values of the period ratio T^*/T_{p1}, more than 3.0. Taking under consideration that, for typical near-fault records, the value of T_{p1} is usually larger than 1.5 s, this improvement concerns only very flexible structures with significantly large period T^*. Therefore, it can be concluded that, in most cases, the use of a 'pulse record' that consists of the two first pulses is adequate. Interesting to note that the minimum errors were observed when the period of the structure T^* was in between the periods of the considered two pulses, T_{p1} and T_{p2}.

CONCLUSIONS

In this study, the effect of the directivity pulses inherent in near-fault ground motions on the inelastic response of a curved RC bridge is investigated. Analyses were performed for a sample of 90 near-fault ground motions, for which the first six significant pulses were identified and extracted. Superposing these pulses sequentially, six synthesized 'pulse records' were constructed for each considered ground motion. NLTH analyses were performed for the original record and the constructed 'pulse records' and for three intensity levels. Thus, conclusions were drawn concerning the accuracy obtained by using the simplified 'pulse records' instead of the original ground motion.

The results show that near-fault phenomena might result in significant amplification of the inelastic response, which maximizes in case of structures with period close to one half the period of the predominant pulse.

Concerning the synthesized 'pulse records', it was found that the predominant pulse alone can predict the inelastic response with acceptable accuracy (error less than 25%) only for structures with period larger than 60% of the period of the pulse and less than twice the pulse period. Outside this range of periods, the addition of the second pulse is usually adequate, except of very flexible structures with period larger than $3T_{p1}$, for which the pulse record must include at least the three first pulses.

ACKNOWLEDGEMENTS

The first author wants to thank the Greek State Scholarships Foundation for the financial support of her postgraduate studies at NTUA through "IKY Fellowships of excellence for postgraduate studies in Greece – Siemens program".

REFERENCES

[1] Shahi, S.K., Baker, J.W. (2011). "An empirically calibrated framework for including the effects of near-fault directivity in probabilistic seismic hazard analysis". Bulletin of the Seismological Society of America, 101(2): 742–755.

[2] Tothong, P., Cornell, C.A. (2006). "Probabilistic seismic demand analysis using advanced ground motion intensity measures, attenuation relationships, and near-fault effects". PEER Report 2006/11. Pacific Earthquake Engineering Research Center, University of California, Berkeley, CA.

[3] Mavroeidis G.P., Papageorgiou A.S. (2003). "A mathematical representation of near-fault ground motions". Bulletin of the Seismological Society of America, 93:1099-1131.

[4] Baker, J.W. (2007). "Quantitative classification of near-fault ground motions using wavelet analysis". Bulletin of the Seismological Society of America, 97:1486-1501.

[5] Mimoglou, P., Psycharis, I.N., Taflampas, I.M. (2014). "Explicit determination of the pulse inherent in pulse-like ground motions". Earthquake Engineering and Structural Dynamics, 43: 2261-2281.

[6] Lu, Y., Panagiotou, M. (2014). "Characterization and representation of strong near-fault ground motions using wavelet-based cumulative pulse extraction". Tenth U.S. National Conference on Earthquake Engineering Frontiers of Earthquake Engineering, Anchorage, Alaska, July 21-25.

[7] McKenna, F., Fenves, G. L., Scott, M. H., and Jeremic, B. (2000). "Open system for earthquake engineering simulation (OpenSees)". Pacific Earthquake Engineering Research Center, University of California, Berkeley, CA.

[8] Menegotto, M., P.E. Pinto (1973). "Method of analysis for cyclically loaded R.C. plane frames including changes in geometry and non-elastic behaviour of elements under combined normal force and bending". Symposium on the Resistance and Ultimate Deformability of Structures Acted on by Well Defined Repeated Loads, International Association for Bridge and Structural Engineering. Zurich, Switzerland: 15-22.

[9] Scott, B.D., Park, R., Priestley, M.J.N. (1982). "Stress-strain behavior of concrete confined by overlapping hoops at low and high strain rates", ACI Journal, 79(1): 13-27.

[10] Popovics, S. (1973). "A numerical approach to the complete stress-strain curves for concrete". Cement and Concrete Research, 3(5), 583-599.

[11] Mander, J.B., Priestley, M.J.N, Park, R. (1988). "Theoretical stress-strain model for confined concrete". Journal of Structural Engineering, ASCE, 114(8), 1804-1826.

[12] Federal Emergency Management Agency (1997). "NEHRP Guidelines for the seismic rehabilitation of buildings". FEMA Publication No. 273, Washington, D.C.

[13] Kardoutsou, V., Mimoglou, P., Taflampas, I., Psycharis, I.N. (2015). "Evaluation and comparison of new methods for the classification of ground motions as pulse-like or non pulse-like". SECED 2015 Conference: Earthquake Risk and Engineering towards a Resilient World, Cambridge, UK, July 9-10.